Int. J. Multiphase Flow Vol. 12, No. 2, pp. 185–202, 1986
Printed in Great Britain.

0301-9322/86 $3.00 + .00

STUDIES ON TWO-PHASE CROSS FLOW PART III: CHARACTERISTICS OF UNSTEADY FLOW BEHAVIOR

M. YOKOSAWA,† Y. KOZAWA, A. INOUE and S. AOKI
Research Laboratory for Nuclear Reactors, Tokyo Institute of Technology, Ohokayama, Meguro-ku, Tokyo, Japan

(*Received* 12 *June* 1984; *in revised form* 29 *March* 1985)

Abstract—Basic characteristics in a two-phase wake flow, in particular, fluctuations of bubble number density, were investigated experimentally using mainly flat plates. New measuring procedures of the periodicity of the bubble number density and of the spatial distribution of the phase-averaged void fraction were developed. The experimental results indicated that two kinds of flow patterns appeared alternately in the wake. Moreover, it was confirmed that one of them corresponded to the Kármán vortex type in a single-phase flow and the other was similar to the twin eddies type which was observed under low Reynolds number ($Re < 10^2$) in the flow. The alternation process of the two flow patterns depended on the shape of obstacles in the cross flow. In case of a cylinder, numbers of the Kármán vortices formed continuously were very few.

1. INTRODUCTION

A two-phase wake flow around a cylinder was studied in parts I and II of our reports, in which the flow was considered to be in steady state. In the wake flow, however, there existed fluctuations of the bubble number density and of the liquid velocity.

The single-phase cross flow around a cylinder is inevitably unsteady flow due to the periodic shedding of the Kármán vortices except for under condition of extremely low Reynolds number, i.e. $Re < 10^2$. According to the investigations on the Kármán vortex in a single-phase flow (Strouhal 1878, Fage & Johansen 1927, Roshko 1954 a,b, Schaefer *et al.* 1959), large fluctuations of velocity and static pressure are induced by the vortices in the wake region behind a obstacle. The characteristics of heat transfer on the surfaces of the obstacle and another body behind the obstacle are severely affected by the vortices (Eckert & Soehngen 1952, Seban 1960, Perkins & Leppert 1962, Brown *et al.* 1962, Galloway & Sage 1967).

About the Kármán vortex in a bubbly two-phase flow, Hulin *et al.* (1982) reported the shedding frequency and the fluctuation of bubble number density at a position in the wake behind the trapezoidal cylinder used for vortex flow meter in single-phase flow. In a two-phase bubbly flow, the intensive fluctuation of bubble number density appears because bubbles are concentrated to the centers of the Kármán vortices. It is considered that this fluctuation may strongly influence the heat transfer on the surface of a body behind the obstacle and then the temperature fluctuation of a heat transfer tube.

The circulation of each vortex behind the bluff body with sharp edges such as a flat plate is stronger than that behind the blunt body such as a circular cylinder. Actually, the fluctuations in the wake were not observed as clearly around a cylinder as around a flat plate. Shedding frequency of the Kármán vortex is characterized by the Strouhal number. For the bluff bodies with sharp edges such as a flat plate, the separation points are always fixed at the sharp edges, and then the Strouhal number is almost constant and independent of the Reynolds number. The Strouhal number for a flat plate is about 0.14 (Roshko 1955). It depends only on the geometrical conditions, i.e. the shape of the body and the flow blockage.

†Present address: Nuclear & Process Engineering Department, Nuclear Project Division, JGC Co., Ohokubo, Kohonan-ku, Yokohama, Kanagawa, Japan.

On the contrary, for the blunt bodies such as a cylinder, the separation angle changes considerably with increasing of the Reynolds number. Therefore, the range of the Reynolds number is divided by the difference among the flow separation mechanisms into three regions which are commonly called subcritical, supercritical and transcritical, respectively. The separation angle and the Strouhal number corresponding to each region hardly change within each region. For a cylinder, the separation angle is 76° for the subcritical type, the flow pattern in the wake in the subcritical region. When the Reynolds number reaches the critical Reynolds number, about 4×10^5, the separation angle retreats to 130°, the value for the supercritical type. Furthermore, as the Reynolds number exceeds the upper transition Reynolds number, about 4×10^6, the angle recovers to 103° for the transcritical type. Corresponding to these changes of the separation angle, the Strouhal number increases from 0.20 through about 0.47, and then decreases to 0.27 eventually (Roshko 1961). Although the whole range of the experimental conditions in this report was included within the subcritical region of the Reynolds number for a cylinder, the transition of flow pattern from the subcritical type in the liquid single-phase flow to the new flow pattern in the two-phase flow (similar to the transcritical type in the single-phase flow with an increase of the mean void fraction in the main flow) was reported in part II, even in the subcritical region. Therefore, the changes of the Strouhal number with increasing of the mean void fraction in the main flow is anticipated. Consequently, also in the two-phase flow, it is expected that the flow behaviors behind a cylinder characterized by the flow patterns in the wake may be more complicated than those behind a flat plate.

In this report, the basic characteristics in the bubbly two-phase wake flow, in particular, fluctuations of the bubble number density, were investigated experimentally using mainly flat plates. New measuring procedures of the periodicity of the bubble number density and of the spatial distribution of the phase-averaged void fraction were developed, and the configuration of the two-phase wake flow was revealed quantitatively. The two-phase flow around a cylinder was discussed again on the basis of these experimental results.

The experimental apparatus and the two-phase main flow conditions were the same as those in part I. Four kinds were selected for the characteristic dimension of the flat plates, i.e. $d = 10, 20, 30$ and 40 mm, which were also the same as of the cylinders. The thickness of the flat plate was 1 mm and both edges were sharpened at angle with 45° from the back side of the plate in order to eliminate the effect of the plate thickness on the wake flow.

2. MEASURING PROCEDURES

The measuring procedures for the fluctuations of the bubble number density is described in this section, but the other procedures can be read in part I or II.

A sensor of gas or liquid phase was a conductivity probe as shown in figure 1. The earth electrode was fixed on the wall of the two-phase flow duct. This probe could be traversed at an arbitrary position (x, y) around the body in the test section. In the output signals of this probe, the liquid-phase signal was cut off in the discriminator, while the gas-phase signal was converted to a rectangular wave using the pulse generator. The probe signal via these two electronic circuits is the void signal $\alpha(x, y; t)$ defined as 1 or 0, that is,

$$\alpha(x, y; t) = \begin{cases} 1, \text{ when a position } (x, y) \text{ is occupied by gas phase,} \\ 0, \text{ when a position } (x, y) \text{ is occupied by liquid phase.} \end{cases} \quad [1]$$

The signal $\alpha(x, y; t)$ was processed in the real-time correlator, and an autocorrelation function $\Phi(x, y; \tau)$ could be finally obtained. When there needs a cross-correlation function $\Phi(x, y; x', y'; \tau)$, two conductivity probes were located at two different positions in the test section, and these two output signals were also processed with the same method as the above-mentioned.

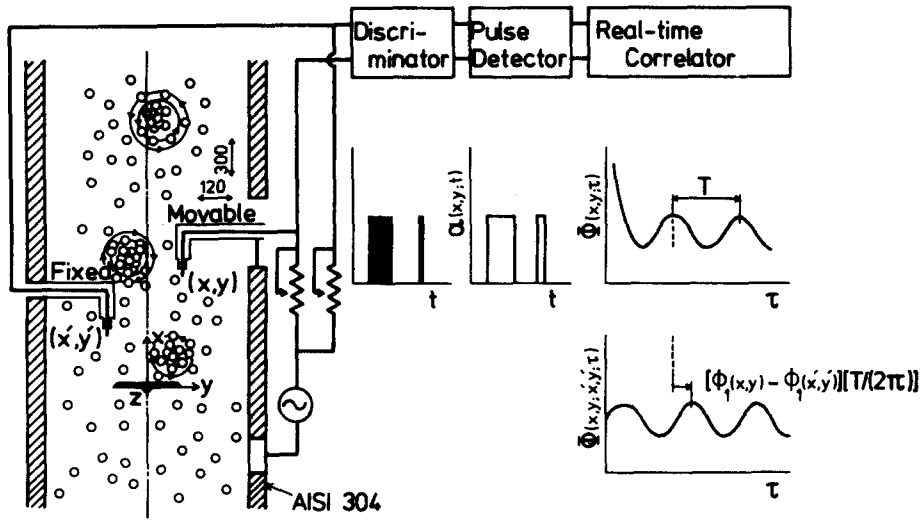

Figure 1. Schematic of phase-averaged void fraction measurement.

If $\alpha(x, y; t)$ has periodicity whose period is T, the phase-averaged void fraction ${}^{p}\overline{\alpha}(x, y; \tau)$ of $\alpha(x, y; t)$ is defined as follows:

$$ {}^{p}\overline{\alpha}(x, y; \tau) = (1/M) \sum_{n=0}^{M-1} \alpha(x, y; \tau + nT), \quad 0 \le \tau \le T, \qquad [2] $$

where M is a positive integral number being sufficiently large. When an another analog signal with fine periodicity is available, Hulin *et al.* (1982), ${}^{p}\overline{\alpha}(x, y; \tau)$ can be obtained directly through the definition, using the analog signal as the triggering one for the averaging. Without the triggering signal, however, ${}^{p}\overline{\alpha}(x, y; \tau)$ could be roughly obtained by means of the only conductivity probes through the following procedures.

${}^{p}\overline{\alpha}(x, y; \tau)$ can be expressed by means of the Fourier series as follows:

$$ {}^{p}\overline{\alpha}(x, y; \tau) = C_0(x, y) + \sum_{n=1}^{\infty} C_n(x, y) \cos [n\omega\tau + \phi_n(x, y)], \qquad [3] $$

where ω is the angular frequency ($\omega = 2\pi/T$), $C_0(x, y)$ is the time-averaged local void fraction ${}^{t}\overline{\alpha}$. The other $C_n(x, y)$ is each amplitude of the fluctuation component with the angular frequency $n\omega$ and is positive. $\phi_n(x, y)$ is each spatial phase-shift of the component. The autocorrelation function, $\Phi(x, y; \tau)$ of $\alpha(x, y; t)$, and the cross-correlation function, $\Phi(x, y; x', y'; \tau)$ of $\alpha(x, y; t)$ and $\alpha(x', y'; t)$, can be approximately described as follows:

$$ \begin{aligned} \Phi(x, y; \tau) &= \overline{{}^{t}\alpha(x, y; t)\alpha(x, y; t - \tau)} \\ &\simeq \overline{{}^{t}{}^{p}\overline{\alpha}\,(x, y; t)\,{}^{p}\overline{\alpha}\,(x, y; t - \tau)} = C_0^2(x, y) + (1/2) \sum_{n=1}^{\infty} C_n^2(x, y) \cos (n\omega\tau). \end{aligned} \qquad [4] $$

$$ \begin{aligned} \Phi(x, y; x', y'; \tau) &= \overline{{}^{t}\alpha(x, y; t)\alpha(x', y'; t - \tau)} \\ &\simeq \overline{{}^{t}{}^{p}\overline{\alpha}\,(x, y; t)\,{}^{p}\overline{\alpha}\,(x', y'; t - \tau)} \\ &= C_0(x, y) \cdot C_0(x', y') + (1/2) \sum_{n=1}^{\infty} C_n(x, y) \\ &\quad \cdot C_n(x', y') \cos \{n\omega\tau + [\phi_n(x, y) - \phi_n(x', y')]\}. \end{aligned} \qquad [5] $$

However, $\Phi(x, y; 0)$ is actually equivalent to ${}^{t}\overline{\alpha}$. As shown in figure 1, the measuring result of $\Phi(x, y; \tau)$ decreased significantly from the value as τ increased, and then the oscillatory

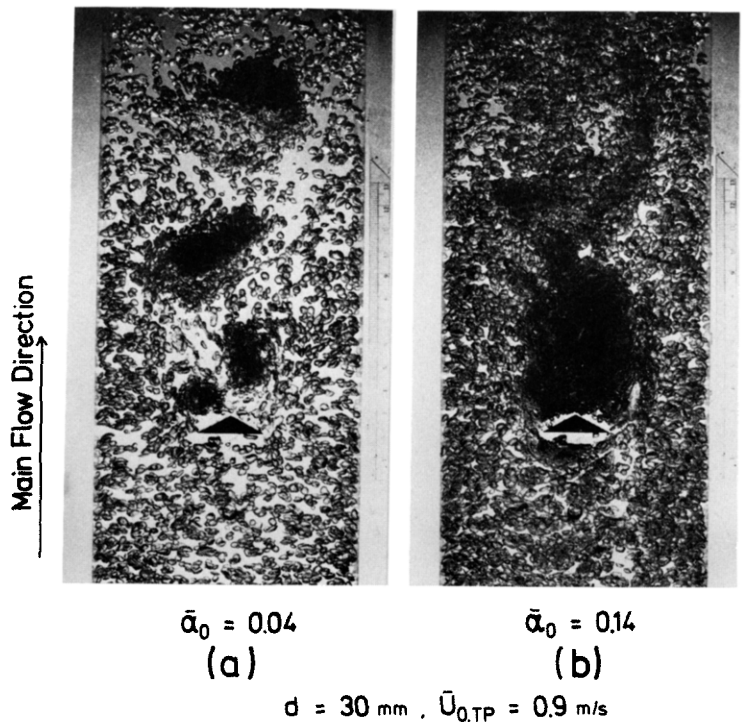

Figure 2. Photographs of bubble behavior in two-phase wake flow around a flat plate.

curve appeared. The oscillatory curve was also observed in the case of $\Phi(x, y; x', y'; \tau)$. The amplitudes of the oscillation became small as τ increased further and $\Phi(x, y; \tau)$ and $\Phi(x, y; x', y'; \tau)$ seemed to reach finally the values, ${}^{t}\overline{\alpha}^{2}(x, y)$ and ${}^{t}\overline{\alpha}(x, y) \cdot {}^{t}\overline{\alpha}(x', y')$, respectively. If the decreasing trend of the oscillation amplitudes are weak and can be ignored, the equations [4] and [5] are considered to be valid except for in the vicinity of $\tau = 0$ in the case of $\Phi(x, y; \tau)$. From the measuring result of $\Phi(x, y; \tau)$, the period T, the time-averaged local void fraction C_0 and each amplitude of the fluctuation component C_n can be determined using equation [4]. Each spatial phase-shift of the component, $[\phi_n(x, y) - \phi_n(x', y')]$, is also obtained from the measuring result of $\Phi(x, y; x', y'; \tau)$ and equation [5].

The only C_0, C_1 and C_2 were distinguishable, because the other amplitudes of the fluctuation components were the same order as the noise level in $\Phi(x, y; \tau)$ due to the irregularity involved in the signal of $\alpha(x, y; t)$. Therefore, the measuring result of ${}^{p}\overline{\alpha}(x, y; \tau)$ from these procedures was the approximate function by means of the first three terms in equation [3]. $[\phi_1(x, y) - \phi_1(x', y')]$ and $[\phi_2(x, y) - \phi_2(x', y')]$ were also distinguished. If ϕ_1 and ϕ_2 at an arbitrary position can be given, the approximate function of the phase-averaged void fraction ${}^{p}\overline{\alpha}(x, y; \tau)$ can be realized.

Besides, C_0 was measured with the same technique as that in our previous reports. When all amplitudes of the fluctuation components was equal to zero, it was decided that there was no periodicity in the fluctuation of the bubble number density.

3. EXPERIMENTAL RESULTS

Figure 2 shows the bubble behavior in the two-phase wake flow behind a flat plate. Black particles in the photographs are bubbles. The unique flow pattern having the periodic fluctuation of the bubble number density was always observed as shown in figure 2(a) when the mean void fraction in the two-phase main flow $\bar{\alpha}_0$ was relatively low. The scale of the fluctuation was related to the plate width d. A portion in which the bubble number density becomes high locally and temporally, as shown in figure 2(a) is named "a bubble crowd." The bubble crowds were created just behind edges of the flat plate alternately and shed to the

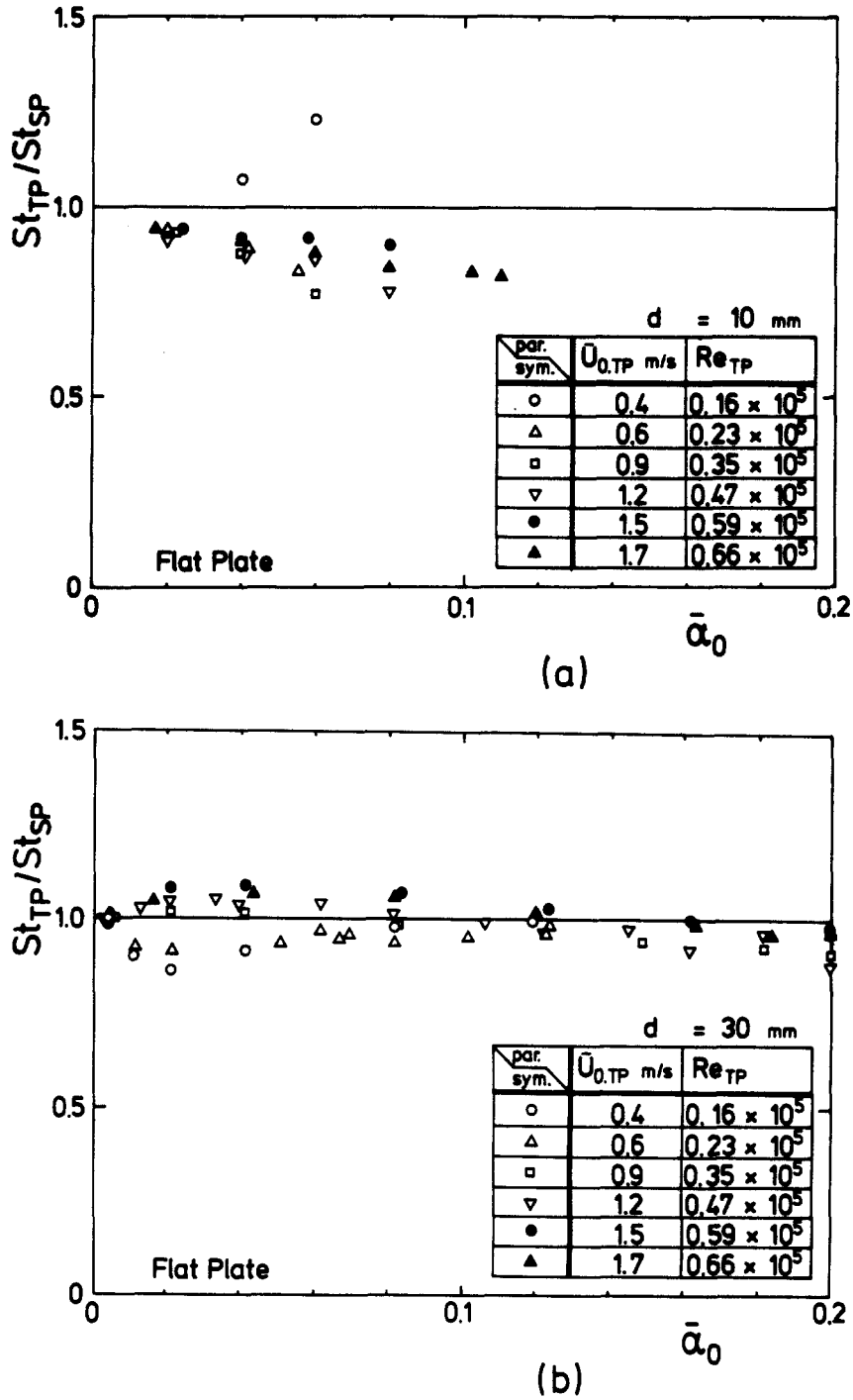

Figure 3. Effect of mean void fraction in main flow $\bar{\alpha}_0$ on Strouhal number of two-phase flow St_{TP} in the case of a flat plate for d = 10 mm (a) and 30 mm (b).

downstream with the regularity similar to the Kármán vortices in single-phase flow. Contrary to the significant concentration of bubble number density within the bubble crowd, the density in the surroundings was somewhat low compared with the value in the main flow, so that the bubble crowd was clearly observed.

When $\bar{\alpha}_0$ increased in excess of a certain value, another flow pattern appeared in the wake and the alternation phenomenon of two flow patterns was observed. This new flow pattern was significantly different from that shown in figure 2(a) and was almost in steady

state. Figure 2(b) corresponds to this flow pattern. The region of the stagnant bubbles whose scale was larger than the bubble crowd shown in figure 2(a) existed behind the plate. This flow pattern was observed only under the alternate changing process of the two patterns and did not appear continuously under any condition of the plate width and the main flow.

The shedding frequency of the Kármán vortex in the liquid single-phase flow was measured with a hot-film anemometer. The frequency was almost in proportion to the mean velocity in the main flow $\overline{U}_{0.TP}$ and the Strouhal numbers for $d = 10$, 20, 30 and 40 mm were 0.11, 0.16, 0.19 and 0.23, respectively. The increasing trend with d is attributed to the flow blockage d/h, where h is the width of the flow duct. The shedding frequency of the bubble crowd could be determined by the periodicity measurements of the bubble number density. The shedding period of the bubble crowd was defined by the same way as that for the Kármán vortex in single-phase flow, i.e. the time within which a pair of the bubble crowds passed through the cross section of the duct. The shedding frequency of bubble crowd under extremely low $\overline{\alpha}_0$ was equal to the value of the Kármán vortex in the single-phase flow within errors ±3%. This fact meant that the formation of the bubble crowd was strongly related to the Kármán vortex. Assuming that the shedding frequency of the bubble crowd f corresponded to that of the Kármán vortex in the two-phase flow, the Strouhal number of the two-phase flow St_{TP} was defined by the following equation.

$$\mathrm{St}_{TP} = fd/\overline{U}_{0.TP}. \qquad [6]$$

Figure 3 shows the effects of the mean void fraction in the main flow $\overline{\alpha}_0$ on the Strouhal number of the two-phase flow. A ratio of the Strouhal number of the two-phase flow St_{TP} to that of the single-phase flow St_{SP} is used in the figure. For $d = 10$ mm, $\mathrm{St}_{TP}/\mathrm{St}_{SP}$ decreases as $\overline{\alpha}_0$ increases. On the other hand, for $d = 30$ mm, $\mathrm{St}_{TP}/\mathrm{St}_{SP}$ is almost unity within errors ±10%. Therefore, for large d such as $d = 30$ mm, the mean velocity of the main flow $\overline{U}_{0.TP}$ can be obtained by the shedding frequency of the bubble crowd f within the errors.

The spatial distribution of the phase-averaged void fraction ${}^{p}\overline{\alpha}$ was measured to visualize such dynamic processes of a bubble crowd as formation and shedding, using the measuring procedures mentioned in the previous section. The phase-shift of the first component $[\phi_1(x, y) - \phi_1(d, d/3)]$ and that of the second one $[\phi_2(x, y) - \phi_2(d, d/3)]$ were measured

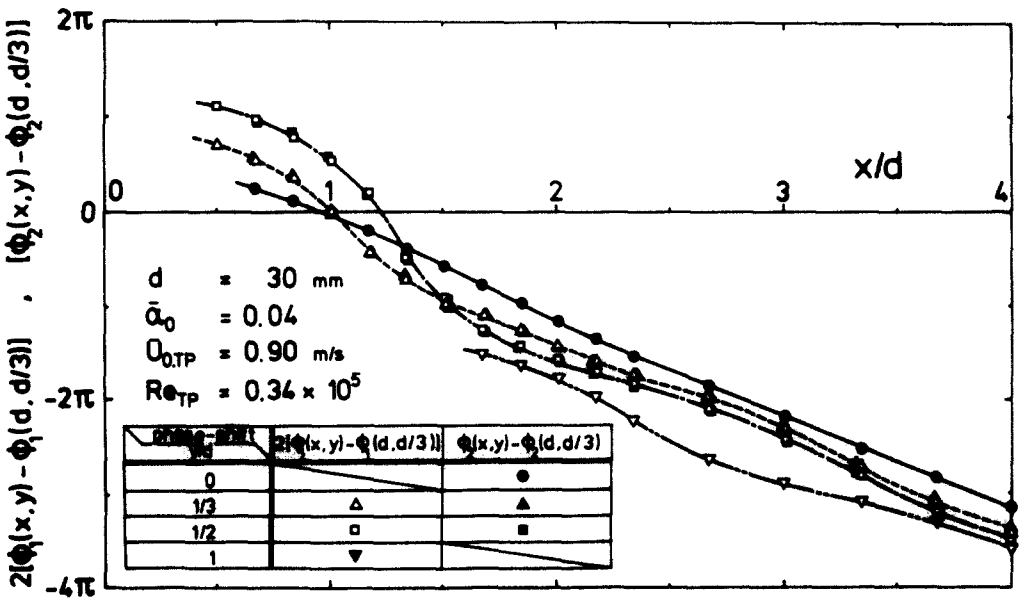

Figure 4. Phase-shifts of fluctuation components, ϕ_1 and ϕ_2, around a flat plate.

as shown in figure 4. The phase shifts were measured separately. When $[\phi_2(x, y) - \phi_2(d, d/3)]$ was measured, the standard point (x', y') was fixed at $(3d,0)$, i.e. $[\phi_2(x, y) - \phi_2(3d,0)]$ was measured, because C_1 was zero and the second term of $\Phi(x, y; x', y'; \tau)$ in [5] vanished on the x-axis. And then $[\phi_1(x, y) - \phi_1(d, d/3)]$ was measured, choosing the standard point at $(d, d/3)$ where $C_1(x, y)$ was almost the largest. The standard point for $\phi_2(x, y)$ in figure 4 was shifted from $(3d, 0)$ to $(d, d/3)$. The figure indicates the following relation.

$$2[\phi_1(x, y) - \phi_1(d, d/3)] = [\phi_2(x, y) - \phi_2(d, d/3)]. \quad [7]$$

C_0, C_1 and C_2 are shown in figure 5(a), (b) and (c), respectively. In the vicinity of the x-axis, C_1 was so much smaller than C_2 that $[\phi_1(x, y) - \phi_1(d, d/3)]$ could not measured. On the other hand, as y/d increased, $[\phi_2(x, y) - \phi_2(d, d/3)]$ became undistinguishable because C_2 decreased. Therefore, [7] was exactly valid only within the range of $1/8 \leq y/d \leq 3/4$. It was feasible that the relation of $[\phi_1(x, y) - \phi_1(d, d/3)]$ and $[\phi_2(x, y) - \phi_2(d, d/3)]$ significantly left equation [7] under the condition of $0 \leq y/d \leq 1/8$ or $y/d \geq 3/4$. However, both C_1 and C_2 under the condition of $y/d \geq 3/4$ and C_1 under the condition of $0 \leq y/d \leq 1/8$ were so small that the final result of ${}^{p}\overline{\alpha}$ was considered to be hardly changed by the relation of $[\phi_1(x, y) - \phi_1(d, d/3)]$ and $[\phi_2(x, y) - \phi_2(d, d/3)]$ under these conditions. Thus, applying

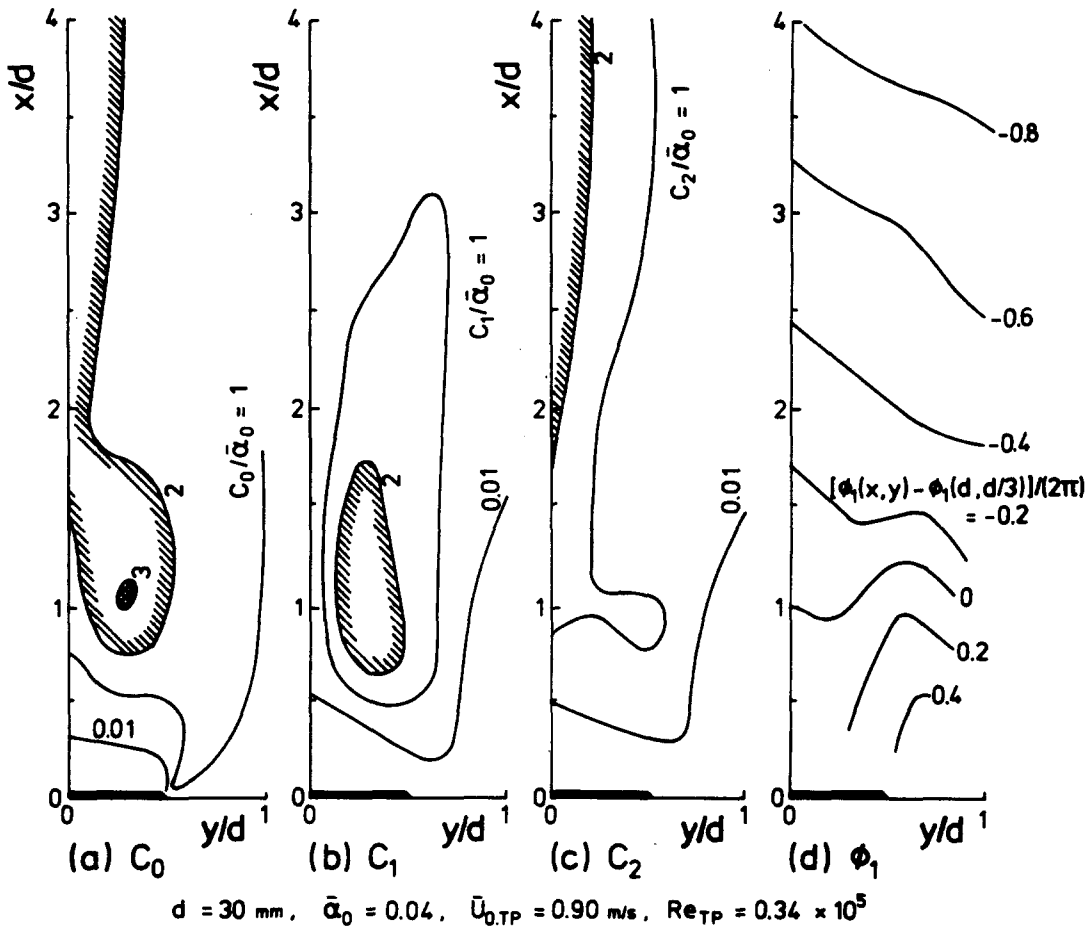

Figure 5. Parameters to represent spatial distribution of phase-averaged void fraction. Time-averaged local void fraction C_0 (a), amplitudes of fluctuation components C_1 (b) and C_2 (c), and phase-shifts of the first fluctuation component ϕ_1 (d).

[7] over the whole range of $y/d \geq 0$, the only $[\phi_1(x, y) - \phi_1(d, d/3)]$ is required to represent ${}^p\overline{\alpha}$. The $[\phi_1(x, y) - \phi_1(d, d/3)]$ under the condition of $0 \leq y/d \leq 1/8$ was obtained from $[\phi_2(x, y) - \phi_2(d, d/3)]$ by means of [7]. The spatial distribution of $[\phi_1(x, y) - \phi_1(d, d/3)]$ is shown in figure 5(d). $\phi_1(d, d/3)$ and $\phi_2(d, d/3)$ in [7] could not be determined in these procedures because $\phi_1(x, y)$ and $\phi_2(x, y)$ were measured as the forms of $[\phi_1(x, y) - \phi_1(x', y')]$ and $[\phi_2(x, y) - \phi_2(x', y')]$. But either $\phi_1(d, d/3)$ or $\phi_2(d, d/3)$ can be fixed at an arbitrary value as follows:

$$\phi_1(d, d/3) = 0. \qquad [8]$$

Figure 6 shows the ${}^p\overline{\alpha}(d, d/3; \tau)$, changing $\phi_2(d, d/3)$ from $-\pi$ to π. Observing the shedding process of the bubble crowds as shown in figure 2(a), the center of the bubble crowd formed behind the edge at $(0, d/2)$ passed the vicinity of $(d, d/3)$. Therefore, when the center passes the cross section of $x/d = 1$, ${}^p\overline{\alpha}(d, d/3; \tau)$ is considered to reach almost the maximum value. After the lapse of about $T/2$, the next bubble crowd formed behind the other edge at $(0, -d/2)$ passes the cross section and ${}^p\overline{\alpha}(d, d/3; \tau)$ undergoes the second largest peak value at the time. Consequently, it was concluded that the following value was appropriate for the $\phi_2(d, d/3)$.

$$\phi_2(d, d/3) = 0, \qquad [9]$$

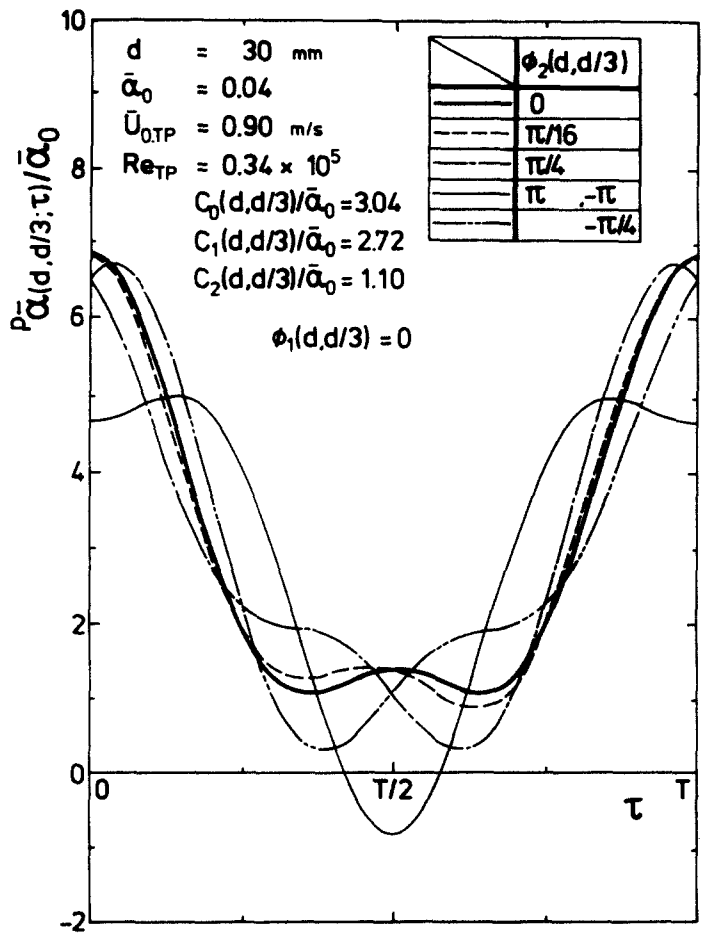

Figure 6. Effect of phase-shift of the second fluctuation component on phase-averaged void fraction at standard point.

where [9] had error within about $\pm\pi/16$ as shown in figure 6. The relation of [7] with [8] and [9] shows that ${}^{p}\overline{\alpha}(x, y; \tau)$ is always represented by the wave shape similar to ${}^{p}\overline{\alpha}(d, d/3; \tau)$ for $\phi_2(d,d/3) = 0$ and is out of phase by $\phi_1(x, y)$ from the ${}^{p}\overline{\alpha}(d, d/3; \tau)$. Besides, C_0, C_1 and C_2 are symmetrical with the x-axis, that is,

$$C_n(x, -y) = C_n(x, y), \qquad [10]$$

and $\phi_1(x, -y)$ is out of phase by π from $\phi_1(x, y)$, i.e.

$$\phi_1(x, -y) = \phi_1(x, y) + \pi \qquad [11]$$

The spatial distribution of the phase-averaged void fraction ${}^{p}\overline{\alpha}(x, y; \tau)$ was finally obtained by means of figure 5 and equations [7]–[11].

Figure 7 illustrates the result of ${}^{p}\overline{\alpha}$. The condition of the figure is the same as that of figure 2(a), so that the only flow pattern with the periodic shedding of the bubble crowd was

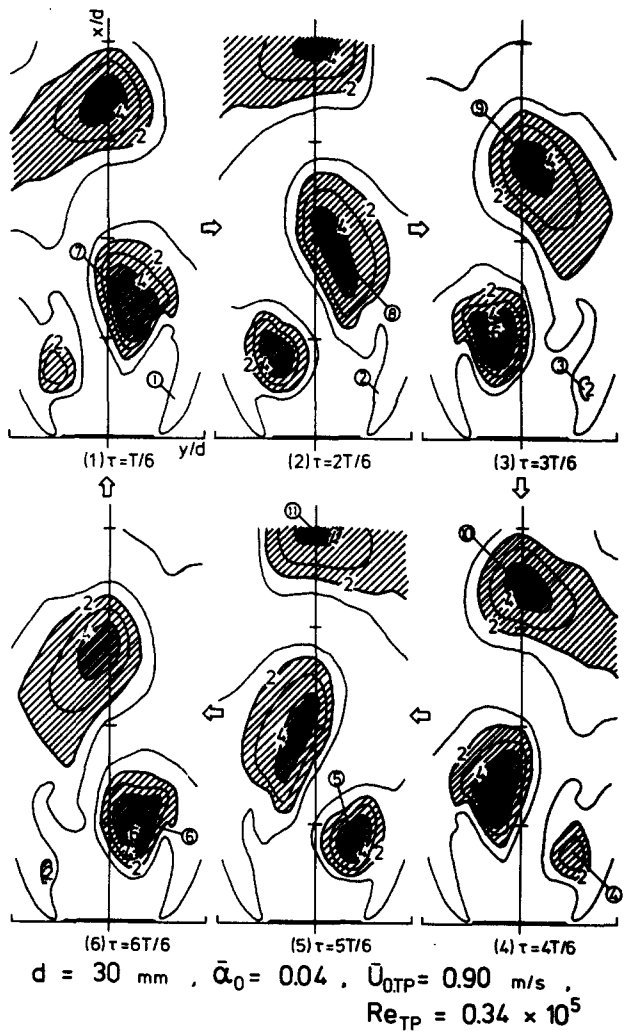

Figure 7. Spatial distribution of ${}^{p}\overline{\alpha}/\overline{\alpha}_0$, phase-averaged void fraction normalized by mean void fraction in main flow, around a flat plate.

always observed. The six pictures represent the change of the spatial distribution of $^{p}\overline{\alpha}$ within a period and the distribution changes from (1) via (2)–(6) by the time $T/6$ to return to (1). Especially, figure 7(2) seems to represent the flow configuration in the photograph shown in figure 2(a). We take successive numbers from ① to ⑪, to explain such behavior of the bubble crowd as creating, growing and shedding. The creating of the bubble crowd corresponds to ② and the bubble crowd is growing from ② through ⑥. It seemed that the formation of the bubble crowd resulted from the accumulation of bubbles at the center of a vortex during the formation process of the Kármán vortex. The bubble number density in the bubble crowd attained a maximum value at the position of $x/d \simeq 1$ and $y/d \simeq 1/4$, and in particular, the density in the center region of the bubble crowd exceeded 6 times of that in the two-phase main flow. Hulin *et al.* (1982) reported a similar value at 170 mm downstream of the trapezoidal cylinder with a width $d = 35$ mm. After the growing process, the bubble crowd is shedding and decays rapidly from ⑥ through ⑪. The bubble concentration within the bubble crowd is ruled in the balance between the accumulation by the centrifugal force of the Kármán vortex and the diffusion into the main flow. Increase of the bubble number density in the bubble crowd not only promotes the diffusion but breaks down the Kármán vortex to weaken the accumulation. Then the bubble crowd decays rapidly in this duration. Thus the flow pattern with the periodic shedding of the bubble crowd shown in figure 2(a) corresponds to the Kármán vortex type in the single-phase flow.

The alternation process of the two flow patterns could be clearly observed in case of a flat plate as illustrated in figure 8 under the condition of low $\overline{U}_{0.TP}$ and relatively high $\overline{\alpha}_0$. Figures 8(a) and (d) correspond to the Kármán vortex type and the flow pattern in steady state, respectively. The transition from (a) to (d) involved the following processes: In the first instance, bubbles clung just behind the liquid single-phase portion on the rear surface of the plate as shown in (b). As this region of the stagnant bubbles grew gradually from (b) via (c) to (d), the scale of the bubble crowd became small and the bubble number density at the center of the bubble crowd also got low. The region behaved as a kind of flow obstacle, and consequently, played such a role as streamlining the flat plate. The disturbance of the bubble number density near the end of the region of the stagnant bubbles in figure 2(b) was caused by the bubble crowd whose scale was considerably small and whose intensity was very low. On the contrary, the transition from (d) to (a) is caused by leaving of the whole region of the stagnant bubbles due to increment of the buoyancy force acting on the stagnant bubbles as illustrated in (e). Therefore, the time duration required for the transition from (d) to (a) was the same order as the shedding period of the bubble crowd T. On the other hand, that from

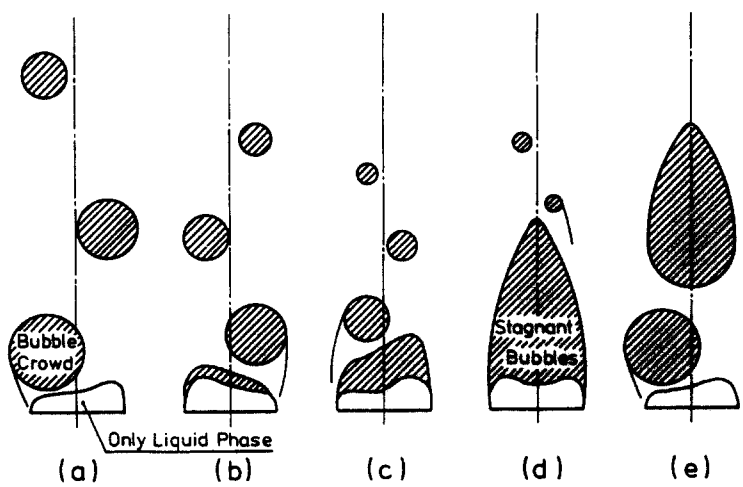

Figure 8. Alternation process of two flow patterns in case of a flat plate.

(a) to (d) was several to tens of times larger than T. The continuation time durations of the Kármán vortex type (a) and the flow pattern in steady state (d) were from the order of T to several hundreds times or sometimes more. Besides, when $\overline{U}_{0.TP}$ was high, the disturbance of the bubble number density near the end of the region of the stagnant bubbles was intensive, the length of the region violently changed, and then, the transition process from (d) via (c) and (b) to (a) was also observed.

The flow pattern in steady state sometimes continued to exist for several hundred times or more than T, as mentioned above. The periodicity in the fluctuation of the bubble number density was measured at the time, but the periodicity such as that of the Kármán vortex could not be detected. In the region of the stagnant bubbles, the circulating behavior of bubbles symmetrical with the x-axis was observed. This fact shows the existence of the stationary twin eddies. Therefore, the flow pattern in steady state is similar to the "twin eddies type" which appears at low Reynolds number ($Re < 10^2$) in a single-phase flow, and it can be considered that high void fraction regions are formed at the centers of the stationary twin eddies by the centrifugal force of those. But the high void fraction regions in figure 5(a) were resultant from the time-averaging over the shedding process of the bubble crowd shown in figure 7, so that there were no stationary twin eddies at the centers of the regions. The region was formed in the balance between the shedding velocity of the bubble crowd and the bubble number density at the center of the bubble crowd. Thus the formation of the high void fraction regions in the spatial distribution of the time-averaged void fraction $\overline{\alpha}$ was caused not only by the centrifugal force of the stationary twin eddies but also by the passage of the bubble crowd.

The measurable range of the shedding frequency of the bubble crowd are shown in figure 9. The boundary in the figure was the condition under which the first peak in the autocorrelation function became unable to be distinguished at any position on the cross section of $x/d = 3$ in the periodicity measurements of the bubble number density. When d was large, the bubble concentration upon the center of the bubble crowd in the Kármán vortex type was high. Therefore, the shedding frequency of the bubble crowd could be measured, if the Kármán vortex continuing for $10T$ or more was detected several times

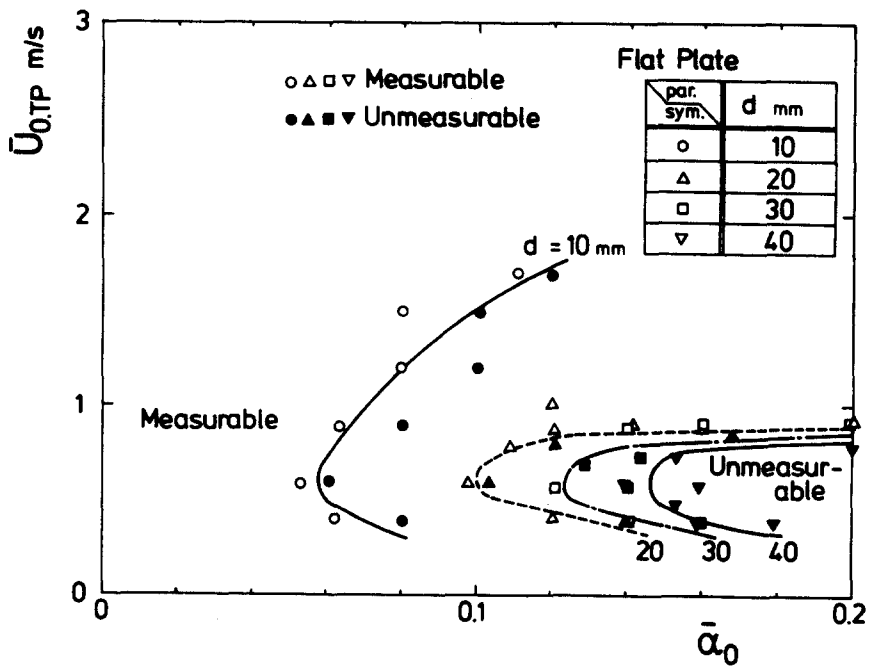

Figure 9. Measurable range of shedding frequency of bubble crowd behind a flat plate.

within the measuring time corresponding to about $1700T$. Considering together that the alternation process shown in figure 8 was observed frequently even in the unmeasurable range, it was shown that the time duration was very short in such a range. When d was small, the bubble concentration was low and consequently the accuracy of the detection of the bubble crowd was low. Therefore, especially for $d = 10$ mm, the time duration of the Kármán vortex type might be long in some degree even in the unmeasurable range. There was the region where the only Kármán vortex type continued stably under the condition of low $\bar{\alpha}_0$. When $\bar{\alpha}_0$ increased in excess of a certain value, the twin eddies type also appeared and the alternation of the two flow patterns was observed. The boundary of the appearance of the twin eddies type had little responsibility. As $\bar{\alpha}_0$ increased further, the time duration and elapsed time ratio seemed to decrease gradually. When $\bar{\alpha}_0$ exceeded the boundary value shown in figure 9, the time duration of the Kármán vortex type became very short but the two flow patterns still appeared alternately. Thus, the boundary in figure 9 represented the condition under which the time duration of Kármán vortex type became very short. Therefore, figure 9 shows the increasing trend of the time duration with the increase of d. This could be considered to be due to the fact that the scale of the Kármán vortex and the value of its circulation increased as d increased, the value became slightly large with an increase of the flow blockage d/h, and that almost all bubbles were carried away by the bubble crowd; consequently, the accumulation of bubbles behind the plate shown in figures 8(b) and (c) was obstructed. For $d \geq 20$ mm, the unmeasurable region was narrow and existed only near the condition $\bar{U}_{0.TP} = 0.6$ m/s, because the buoyancy force acting on the stagnant bubbles was relatively large under low $\bar{U}_{0.TP}$ condition and the transition from (d) via (c) and (b) to (a) in figure 8 was also appeared under high $\bar{U}_{0.TP}$ condition.

4. CONSIDERATIONS

Let us consider the wake flow behind a cylinder, referring to the abovementioned experimental results of a flat plate.

As reported previously (in parts I and II), when d was small and $\bar{\alpha}_0$ was relatively low, the bubble crowd seemed to be shed periodically, but it was not so clear as that behind a flat plate. When d became large and $\bar{\alpha}_0$ increased, the wake flow became almost in steady state and shifted to the other flow pattern. Thus, in case of a cylinder, there also seemed to exist the two kinds of flow patterns.

The Strouhal number St_{SP} in the case of a cylinder for $d = 10$, 20, 30 and 40 mm were 0.16, 0.18, 0.20 and 0.22, respectively. Figure 10 shows the effects of $\bar{\alpha}_0$ on the Strouhal number of the two-phase flow St_{TP}. For $d = 10$ mm, St_{TP}/St_{SP} decreases as $\bar{\alpha}_0$ increases. This trend is weak for $d = 30$ mm. Thus the flow pattern with shedding of the bubble crowd corresponds the Kármán vortex type in the case of a flat plate shown in figure 2(a).

Both of the new flow pattern and the twin eddies type in the case of a flat plate are almost in steady state without the shedding of the bubble crowd and have the stationary regions of the stagnant bubbles in the wake. As reported in our first report, the new flow pattern had a special feature of a pair of high void fraction regions not only in the wake but also near the cylinder surface; in particular, the latter regions considerably affected the two-phase flow behavior in the wake. The formation of the high void fraction regions is caused not only by the centrifugal force of the stationary twin eddies but also by the passage of the bubble crowd, as mentioned in section 3. As reported in our second report, the distribution of the static pressure on the cylinder surface Cp_{sur} shifted from the subcritical type in the single-phase flow to the new one in the two-phase flow with increasing of d and $\bar{\alpha}_0$. The new type was similar to the transcritical one in the single-phase flow. Accordingly, the flow pattern of the Kármán vortex type has the distribution of Cp_{sur} similar to the subcritical type in the single-phase flow and the new flow pattern has the distribution similar to the transcritical one. The transcritical type in a single-phase flow is also unsteady flow with the

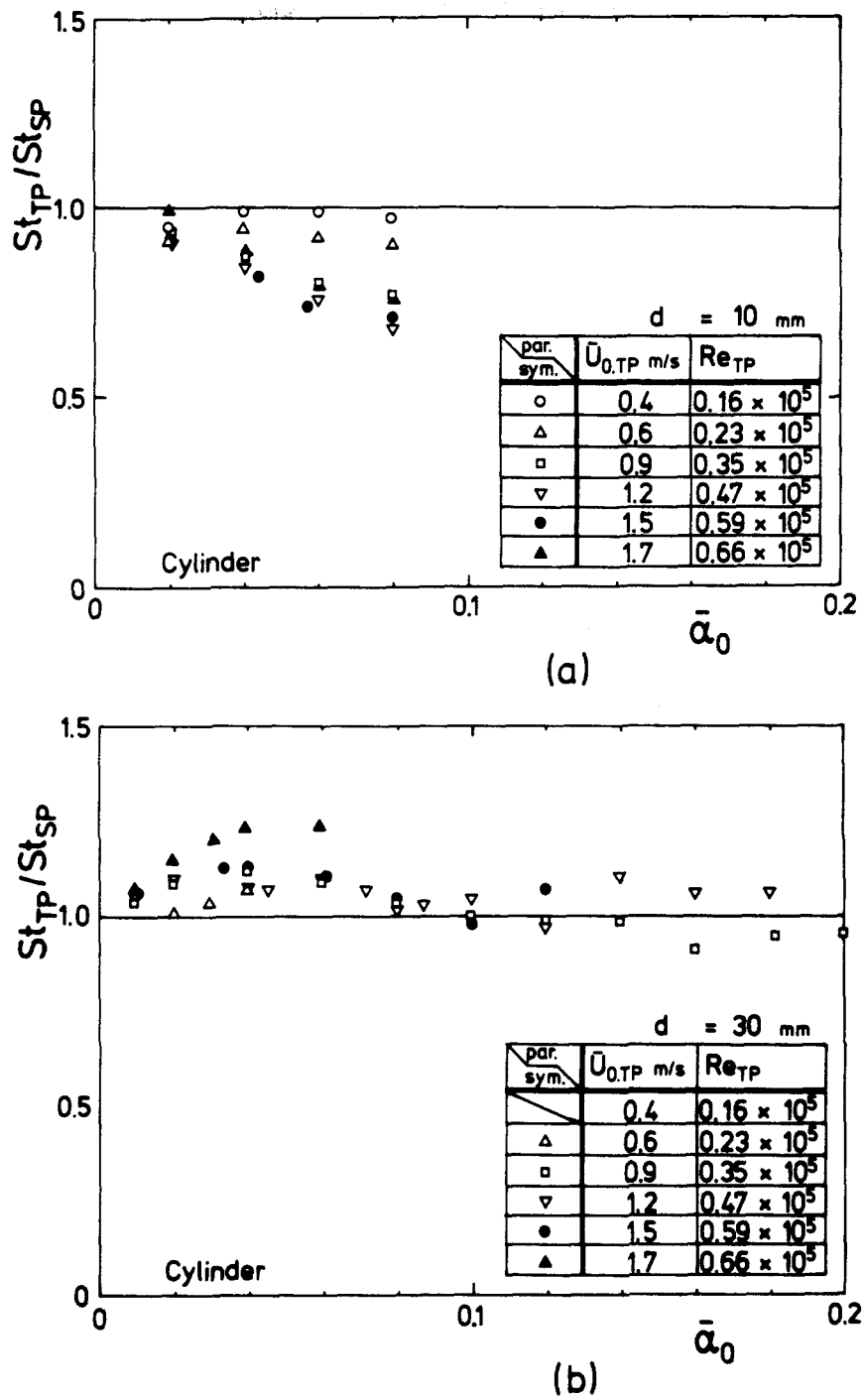

Figure 10. Effect of mean void fraction in main flow $\bar{\alpha}_0$ on Strouhal number of two-phase flow St_{TP} in the case of a cylinder for d = 10 mm (a) and 30 mm (b).

shedding of the Kármán vortex. If the new flow pattern corresponds to the transcritical type in the single-phase flow, the ratio of the Strouhal number St_{TP}/St_{SP} for large d is expected to increase to reach about 1.4 as $\bar{\alpha}_0$ increases. But St_{TP}/St_{SP} seems to reach about unity. Compared with the subcritical type, both the circulation of the vortex and its scale for the transcritical type are small. Furthermore, the periodicity is weak, while the shedding frequency is large. Therefore, the periodicity of the bubble number density for the transcritical type may be unable to be detected even though the formation of the high void fraction regions in the wake is caused by the passage of the bubble crowd. However, it is

considered that the bubble crowd can be neglected and that there is no large difference between the wake flow in this case and that in the case of a flat plate, because the bubble crowd is so faint. This flow pattern, therefore, can be regarded as that similar to the twin eddies type.

As mentioned above, there also exist the two flow patterns in the case of a cylinder. One of them is the Kármán vortex type and the other is similar to the twin eddies type. The transition process of these flow patterns, however, was not clear at all. The autocorrelation function at a position on the center axis of the Kármán vortex row was measured as shown in figure 11. The oscillation amplitude of the function for a cylinder becomes small as τ increases under the condition of $d = 30$ mm where the accuracy of the detection of the bubble crowd is high, while the trend for a flat plate is weak. This fact shows that the flow patterns in the case of a cylinder change by turn as in the case of a flat plate. Now, the elapsed time ratio of the Kármán vortex type can be calculated under the following assumptions:

1. When the Kármán vortex type appears in the wake, definite number of the Kármán vortex are produced continuously.
2. The time duration of the twin eddies type is quite random.

The phase-average void fraction ${}^{p}\bar{\alpha}$ of the Kármán vortex type and of the twin eddies type at the position of $x/d = 3$ and $y/d = 0$ can be described as follows:

$$ {}^{p}\bar{\alpha} = A + B \cos 2\omega\tau; \quad \text{for the Kármán vortex type,} \qquad [12] $$

$$ {}^{p}\bar{\alpha} = C; \quad \text{for the twin eddies type,} \qquad [13] $$

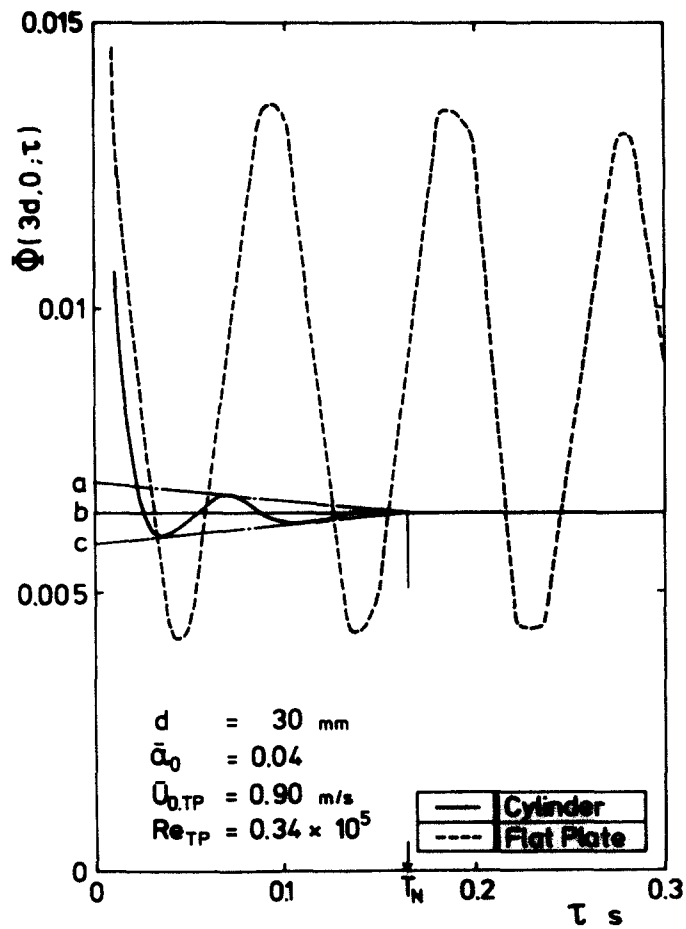

Figure 11. Autocorrelation function at a position on center axis of Kármán vortex row.

where ω is the angular frequency of the bubble crowd. In [12], the term corresponding to the first fluctuation component in [3] is zero because of the condition $y/d = 0$. When R is the elapsed time ratio of the Kármán vortex type and N is the number of the Kármán vortices formed continuously until the Kármán vortex type is replaced by the twin eddies type, the following relations are obtained:

$$a = (A^2 + B^2/2)R + C^2(1 - R), \quad [14]$$

$$b = (\overline{'\alpha})^2 = [AR + C(1 - R)]^2, \quad [15]$$

$$c = (A^2 - B^2/2)R + C^2(1 - R), \quad [16]$$

$$T_N = NT, \quad [17]$$

where T is the shedding period of the bubble crowd. The values of a, b, c and T_N can be determined as shown in figure 11. N can be calculated using [17]. Figure 12(a) shows the calculation results. Besides, the following equation is obtained by the [14] and [16].

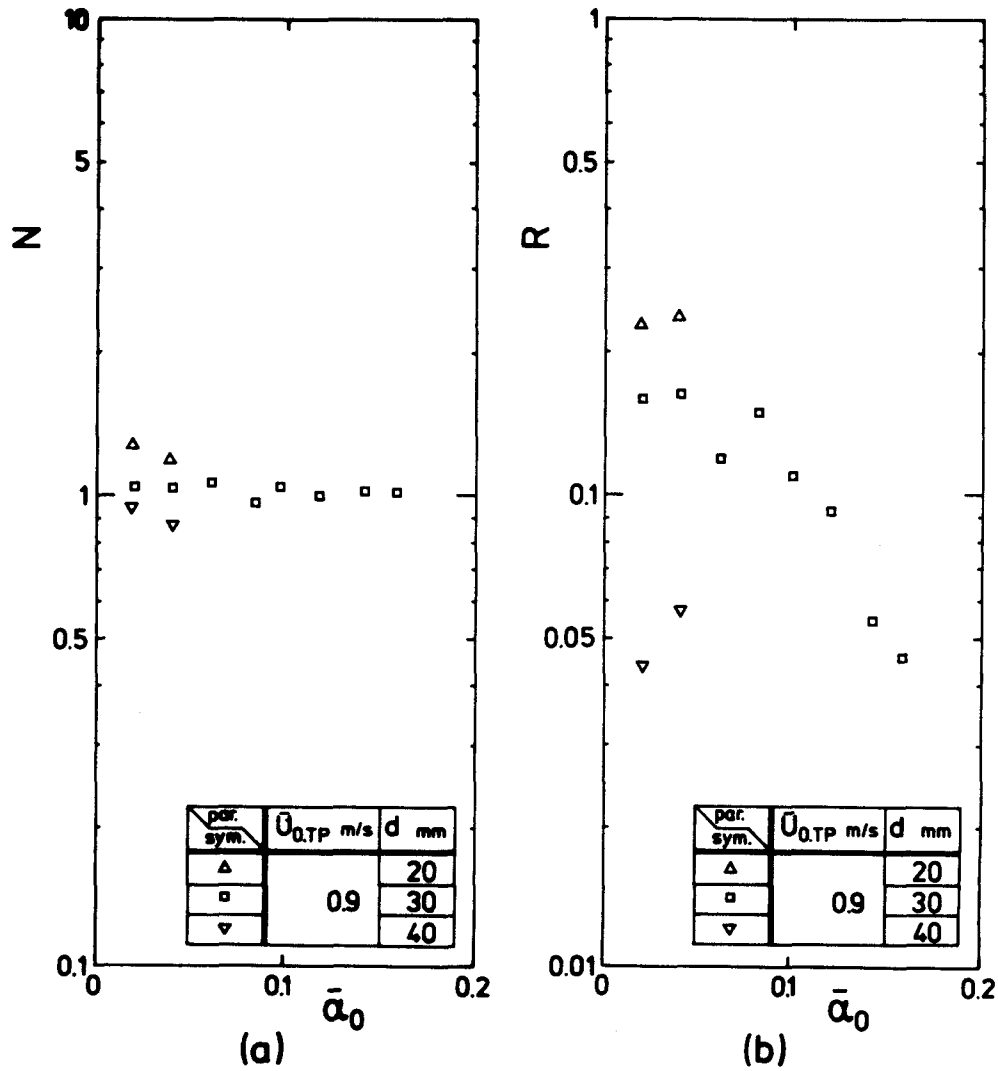

Figure 12. Number of Kármán vortices formed continuously (a) and elapsed time ratio of Kármán vortex type (b), in the case of a cylinder.

$$R = (a - c)/B^2. \quad [18]$$

Using this equation, the elapsed time ratio of the Kármán vortex type for a cylinder R is roughly deduced from substituting $B/\bar{\alpha}_0$ which was measured in almost the complete Kármán vortex type behind the flat plate under the condition of $d = 30$ mm, $\bar{\alpha}_0 = 0.04$ and $\bar{U}_{0.TP} = 0.9$ m/s shown in figure 5(c). The value of $B/\bar{\alpha}_0$ was almost unity, i.e. 0.96. Figure 12(b) shows the relation between R and $\bar{\alpha}_0$ for several diameters of the cylinders. When d is small, the scale of the bubble crowd is small and consequently the accuracy of the detection of the bubble crowd is low. As $\bar{\alpha}_0$ increased, the value of $B/\bar{\alpha}_0$ decreased because the decaying process of the bubble crowd was promoted. Furthermore, it was observed that the ratio of the distance between the rows of the bubble crowd to d increased as d decreased. For $d = 10$ mm, in particular, the periodicity of the bubble number density was not detected on the x-axis. Therefore, it can be considered that $B/\bar{\alpha}_0$ should decrease significantly with a decrease of d. The smaller d is or the higher $\bar{\alpha}_0$ is, the smaller N and R shown in figures 12(a) and (b) are calculated from the actual. The dependency of d on the results should be represented weaker and that of $\bar{\alpha}_0$ should be represented somewhat stronger than the actual. Figure 12(a) means that the Kármán vortices formed continuously are very few. The time duration of the Kármán vortex type becomes short with increasing of d, as shown in figure 12(b). R has a decreasing trend with increasing of $\bar{\alpha}_0$ as well as d. These results of R mean that the two-phase weak flow changes gradually from the complete Kármán vortex type ($R = 1$) to the complete twin eddies type ($R = 0$) with increasing of d or $\bar{\alpha}_0$. This flow pattern changing in the wake flow seems to correspond to decreasing of the drag coefficient ratio $Cd_{Tp}/(Cd_{SP})_{Sub}$ like the experimental results in part II, because the drag coefficient of the twin eddies type is smaller than that of the Kármán vortex type. Since N is a very small number, the flow pattern in the wake flow might be subject to the circumferential conditions for the formation of the Kármán vortices. For example, the decreasing of the liquid layer thickness or the increasing of the local void fraction in the vicinity of the cylinder surface under the conditions of large d and of high $\bar{\alpha}_0$ makes it easy to break down the Kármán vortices during the formation process. Moreover, the high void fraction region near the cylinder surface affects strongly the life time of the Kármán vortex type, too. Thus, the alternation process of the flow patterns in the case of a cylinder might be quite random, and does not have any regularity as in the case of a flat plate.

Figure 13 shows the measurable range of the shedding frequency of the bubble crowd in the case of a cylinder. For large d, the duration time, in which the Kármán vortex was observed, is fairly short in the unmeasurable range. But, for small d, the duration time may be long in some degree even in the unmeasurable range. The bubble number density near the center of the bubble crowd increased with an increase of d, so that the measurable range should become wider with d. However, the range for $d = 30$ mm is considerably wider than those for $d = 20$ and 30 mm, because both the duration time and elapsed time ratio of the Kármán vortex type decreases with the increase of d as shown in figures 12(a) and (b). The range for $d = 10$ mm, which is wider than that for $d = 20$ mm, is not consistent with this trend. Also in part II, the drag coefficient ratio $Cd_{TP}/(Cd_{SP})_{Sub}$ for $d \leq 10$ mm was correlated by the formula different from that for $d = 20 \sim 40$ mm. For $d \leq 10$ mm, therefore, further investigation is considered to be necessary. Thus, the measurable range shown in figure 13 does not correspond to the elapsed time ratio of each flow patterns. And, unlike the case of a flat plate, the range does not correspond to the continuation time duration of the Kármán vortex type.

5. CONCLUSIONS

In the two-phase wake flow around the bodies there existed two flow patterns. They repeated alternate formation. One of them had periodic characteristics for the bubble

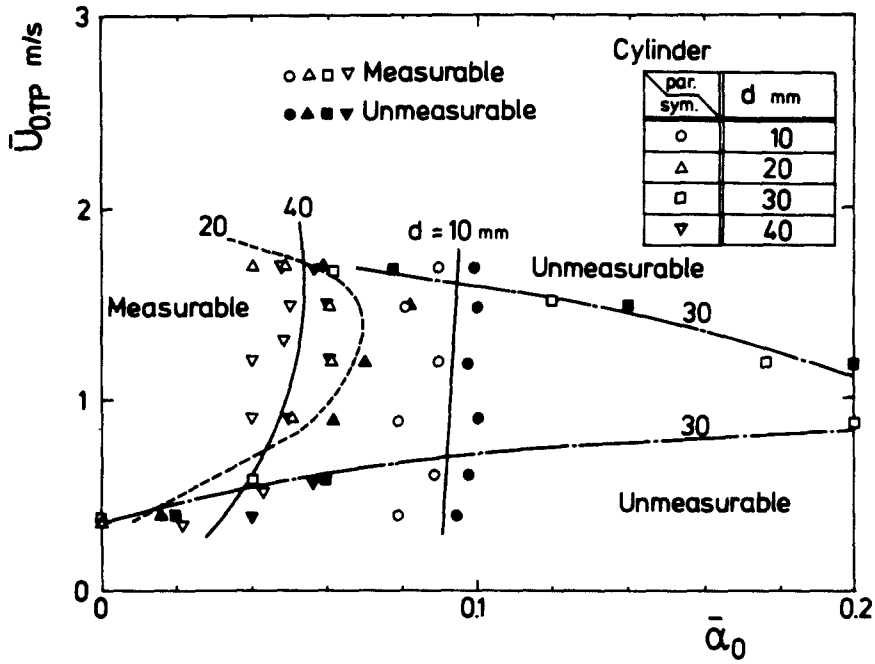

Figure 13. Measurable range of shedding frequency of bubble crowd behind a cylinder.

number density and for the liquid velocity. The period was identical with that of the Kármán vortex and this flow pattern corresponded to the Kármán vortex type in the liquid single-phase flow. Bubbles were accumulated at the center of the Kármán vortex by the centrifugal force of it. On the other hand, the other flow pattern was almost in steady state. The elapsed time ratio of the Kármán vortex type generally decreased with the increase of the mean void fraction in the main flow.

In case of a flat plate, when the mean void fraction in the main flow was relatively low, the only Kármán vortex type continued stably. When the mean void fraction increased to exceed a certain value, the flow pattern in steady state also appeared. But there was almost no repeatability in the condition under which the flow pattern in steady state began to appear and in the continuation time duration of each flow patterns. The flow pattern in steady state was similar to the twin eddies type observed under low Reynolds number ($Re < 10^2$) in the single-phase flow.

In case of a cylinder, the elapsed time ratio of the Kármán vortex type gradually decreased with the increase of the cylinder diameter as well as the mean void fraction in the main flow. This trend was confirmed quantitatively by a rough estimation method. Decreasing the drag coefficient in part II corresponded to decreasing the elapsed time ratio of the Kármán vortex type. The flow pattern in almost steady state might be similar to the transcritical type in the single-phase flow. However, the flow pattern could be regarded as the twin eddies type like in the case of a flat plate, because the periodic characteristics were very faint.

REFERENCES

BROWN W., RITTS, C. C. & LEPPERT, G. 1962 Forced convection heat transfer from a uniformly heated sphere. *ASME J. Basic Engng.* **84,** 133–140.

ECKERT, E. R. G. & SOEHNGEN, E. 1952 Distribution of heat transfer coefficients around circular cylinders in crossflow at Reynolds numbers from 20 to 500. *ASME J. Basic Engng.* **74,** 343–347.

FAGE, A. & JOHANSEN, F. C. 1927 The flow around a cylinder. *Proc. Roy. Soc. London* **A 116,** 170–197.

GALLOWAY, T. R. & SAGE, B. H. 1967 Local and macroscopic transport from a 1.5-in. cylinder in a turbulent air stream. *AIChE J.* **13,** 563–570.

HULIN, J-P., FIERFORT, C. & COUDOL, R. 1982 Experimental study of vortex emission behind bluff obstacles in a gas liquid vertical two-phase flow. *Int. J. Multiphase Flow* **8,** 457–490.

PERKINS, H. C. & LEPPERT, G. 1962 Forced convection heat transfer from a uniformly heated cylinder. *ASME J. Basic Engng.* **84,** 257–263.

ROSHKO, A. 1954a On the development of turbulent wakes from vortex streets. *NACA TR 1191.*

ROSHKO, A. 1954b A new hodograph for free streamline theory. *NACA TN 3168.*

ROSHKO, A. 1955 On the wake and drag of bluff bodies. *J. Aero Space Sci.* **22,** 124–132.

ROSHKO, A. 1961 Experiments on the flow past a circular cylinder at very high Reynolds number. *J. Fluid Mech.* **10,** 345–356.

SCHAEFER, J. W. & ESKINAZI, S. 1959 An analysis of the vortex street generated in a viscous fluid. *J. Fluid Mech.* **6,** 241–260.

SEBAN, R. A. 1960 The influence of free stream turbulence on the local heat transfer from cylinder. *ASME J. Basic Engng.* **82,** 101–107.

STROUHAL, V. 1878 Über eine besondere art der tonerregung. *Ann. Phys. Chem.* **5,** 215–251.